Dynamical diffraction in electron-energy-loss spectrometry: The independent Bloch-wave model

P. Schattschneider* and B. Jouffrey
École Centrale Paris, Laboratoire de Mécanique, Sols, Structures et Matériaux, Grande Voie des Vignes, F-92295 Châtenay-Malabry, France

M. Nelhiebel
Institut für Angewandte und Technische Physik der Technische Universität Wien, A-1040 Vienna, Austria
(Received 11 December 1995; revised manuscript received 5 March 1996)

The double-differential cross section for inner-shell ionization in a crystal by fast electrons is calculated within the theory of dynamical electron diffraction. Bloch waves are used for the incident and the emerging electrons. We show that interference terms are still present in the independent Bloch-wave model. In the two-beam case, the cross section contains but six terms, three of them caused by interference. From the six terms, three are identified as the Kikuchi excess and defect lines and the Kikuchi band. The remaining three terms have not yet been described explicitly. As an example, the Si *K*-shell ionization cross section is calculated for a (220) two-beam case, in a dipole approximation for the mixed dynamic form factor. It is shown that in electron spectroscopic diffraction the maximum of the fundamental Lorentzian can be significantly shifted with respect to the direction of incidence, and that the interpeak minimum between the fundamental and the Bragg-excited Lorentzians is depressed relative to the kinematical case. [S0163-1829(96)02026-7]

I. INTRODUCTION

The understanding of how inelastic scattering of fast electrons combines with dynamical diffraction in a crystal becomes increasingly important with the availability of energy filters in electron microscopy. Predictions of inelastic cross sections in a crystal are important because atomic models for inner-shell ionization cross sections are so accurate nowadays[1] that dynamical effects set up by the crystalline environment should no longer be neglected. Apart from an understanding of the combined elastic-inelastic interactions, calculations would improve the accuracy of quantitation in electron-energy-loss spectrometry (EELS).

Reimer[2] has given a qualitative illustration of the fundamental principles that lead to the formation of Kikuchi lines and bands in energy-filtered diffraction patterns [energy spectroscopic diffraction (ESD)]. A quantitative prediction of ESD patterns for arbitrary energy loss and specimen has yet to be found. However, there has been considerable progress in the last decades, using various approximations related to the wave functions of the fast probe electron and the target, as well as to the interaction, in order to achieve practical solutions.

Kainuma[3] has calculated intensity profiles across Kikuchi lines and bands in a single inelastic-scattering approximation. Later on, various scattering mechanisms were investigated. There are many papers on thermal diffuse scattering[4–8] and on inner-shell excitation.[9–12] Plasmon scattering has been discussed by Howie.[13]

Multiple inelastic scattering has been considered by Yoshioka,[14] and then by Rez,[15] by Van Roost and Serneels in a matrix formulation,[16] and by Dudarev, Peng, and Whelan in a propagator approach.[18]

Although Kainuma realized the symmetry between the incident and the outgoing waves in the formulation of the problem, he assumed a Bloch-wave field only for the outgoing electron, the incident electron being a plane wave. Later work concentrated largely on special cases such as kinematic conditions for the incident[19,20] or the outgoing beam.[10] Of the more general treatments, we mention the papers by Gjønnes,[21] Van Roost and Serneels,[16] and Dudarev *et al.*[18] Despite their general applicability and usefulness, these approaches have not been exploited as they deserve, due to the fact that the average user is not willing to repeat lengthy computer calculations. What is missing is a simple expression that can be handled within reasonable time on reasonable hardware.

This is the aim of the present paper. The aspects of our approach are use of the dipole approximation and reduction of the number of terms to six in the final expression. This allows simulation of ESD patterns on a PC.

The paper is organized as follows: First, we derive an expression for the differential cross section for inelastic scattering in a crystal. Results are derived in distorted-wave Born approximation (DWBA),[22] using Bloch waves for the incident and emerging fast electrons.

Strictly speaking, the eigenfunctions in a system with inelastic interactions are no longer Bloch waves. This case was treated by Dudarev *et al.*[18] We adopt a simpler model system where only core excitations occur. When selecting a core loss in a diffraction pattern, all other inelastic interactions might then be treated as a phenomenological absorption. For the present calculations, we assume single inelastic scattering for core losses and neglect absorption. This allows the specimen thickness $d \to \infty$, leading to a transparent and clear formulation of the problem. It is shown that this approximation is equivalent to the independent Bloch-wave model (IBWM). The effects of finite thickness and absorption will

be discussed in a forthcoming paper.

Following the notation of Kohl and Rose,[23] the use of the mixed dynamic form factor allows a transparent formulation. To this point, results are valid for any energy-loss process. It turns out that in the limit of the validity of the independent Bloch-wave model, interference survives, contrary to earlier conjectures.[10] The validity and limitations of this assumption are discussed.

Thereafter, we invoke a two-beam case for both the incident and the outgoing Bloch-wave superpositions; and we evaluate the mixed dynamic form factor for inner-shell ionization in dipole approximation.[24,25]

These simplifications lead to a transparent description of the inelastic differential scattering cross section. It reduces to a linear combination of six mixed dynamic form factors (three direct and three mixed terms) that can easily be handled. The six coefficients in the linear combination mentioned above are then simple algebraic expressions containing nothing but the excitation errors of the incident and the outgoing waves. From the six terms, three are identified as the Kikuchi excess and defect lines and the Kikuchi band. The remaining three factors have not yet been described explicitly.

In the last section we discuss their physical significance as well as several consequences of our result.

II. GENERAL THEORY

A. Distorted-wave Born approximation

The double-differential scattering cross section for inelastic scattering in the DWBA is

$$\frac{\partial^2\sigma}{\partial\varepsilon\,\partial\Omega}=(2\pi)^4 a_0^{-2}\frac{k}{k_0}\sum_i p_i \times\sum_f |\langle\psi_{\mathbf{k}}|\langle f|V(\mathbf{r}-\mathbf{R})|i\rangle|\psi_{\mathbf{k_0}}\rangle|^2\delta(\omega_{f,i}-\varepsilon), \tag{1}$$

with $\psi_{\mathbf{k_0}}$ and $\psi_{\mathbf{k}}$ the initial and final fast-electron waves, respectively. f,i denote the final and initial states of the scatterer, with occupation probability p_i of initial states. The interaction term in the Hamiltonian is e^2V with $V(\mathbf{r}-\mathbf{R})=|\mathbf{r}-\mathbf{R}|^{-1}$, the Coulomb interaction between the fast electron at $\mathbf{r}$, and the target electron at $\mathbf{R}$. $\omega_{f,i}=\omega_f-\omega_i$ is the energy difference between final and initial states of the scatterer.

The δ function selects those combinations of initial and final states in the double sum that are apart by an energy exactly matching the energy loss ε of the fast electron. Note that the sum over i means that the scatterer is in a mixed state, a consequence of the one-electron approximation.

The fast-electron wave functions $\psi_{\mathbf{k},\mathbf{k}_0}$ are Bloch waves. In configuration space, neglecting spin, the initial state is

$$\psi^{(+)}_{\mathbf{k}_0}(\mathbf{r})=\langle\mathbf{r}|\psi_{\mathbf{k}_0}\rangle=\sum_{g,j} a_j C_g^j e^{i\mathbf{k}^j_{0g}\mathbf{r}}. \tag{2}$$

The final state is[26]

$$\psi^{(-)}_{\mathbf{k}}(\mathbf{r})=[\psi^{(+)}_{-\mathbf{k}}(\mathbf{r})]^* \tag{3}$$

and can be rewritten[27]

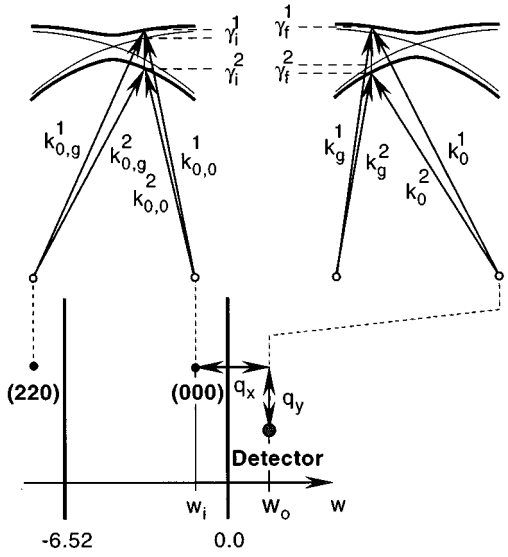

FIG. 1. Scattering geometry with incident beam (000) and detector position in the two-beam case (here, without restriction of generality, Si 220). The position of the Kikuchi lines is drawn. The lines occur at $w_o=0$, $w_o=-6.52$. Scattering vectors are measured with respect to the incident beam; the relation between w_i, w_o, q_x can be seen. The upper part shows the dispersion surfaces for incident and outgoing directions (not to scale), with γ_i^j. See text after Eq. (14) for explanation.

$$\psi_{\mathbf{k}}(\mathbf{r})=\langle\mathbf{r}|\psi_{\mathbf{k}}\rangle=\sum_{h,l} b_l D_h^{l*} e^{i\mathbf{k}_h^{l*}\mathbf{r}}. \tag{4}$$

The wave vector $\mathbf{k}^j_{0g}$ is that of Bloch wave j to Bragg reflexion g in the incident-wave field, and $\mathbf{k}_h^l$ is analogous for the outgoing-wave field, that is, the latter is defined by the selection of an outgoing direction (see Fig. 1).

C_g^j are the expansion coefficients of the jth Bloch wave of the incident-wave field as given by the solution of the characteristic equation of dynamical diffraction theory.[28,29] The respective quantities D_h^l in Eq. (4) refer to the Bloch-wave field after inelastic interaction. This is Kainuma's ''reciprocal wave.'' The wording comes from the fact that the emerging wave field is defined by choice of an exit direction, i.e., by positioning the detector in the diffraction plane, in much the same way as the incident-wave field is defined by the position of the electron source. According to Eq. (3), D_h^l are obtained as the Bloch-wave coefficients of $\psi^{(+)}_{-\mathbf{k}}(\mathbf{r})$. The coefficients a_j, b_l can be calculated as usually in dynamical diffraction theory from the boundary conditions at the upper and lower boundaries of the specimen as

$$a_j=C_0^{j*}$$

for $z=0$ and

$$b_l=D_0^l e^{-i\gamma^{l*}d}$$

for $z=d$. See Fig. 1 and Eq. (14) for a definition of γ^l.

Double insertion of the unity operator

$$1=\int d^3r|\mathbf{r}\rangle\langle\mathbf{r}| \tag{5}$$

for the configuration space variable of the fast electron into Eq. (1), evaluation of the square, and use of Eqs. (2), (4) yields

$$\frac{\partial^2\sigma}{\partial\varepsilon\,\partial\Omega}=(2\pi)^4 a_0^{-2}\frac{k}{k_0}\sum_{g,j} a_j C_g^j \sum_{g',j'} a_{j'}^* C_{g'}^{j'*} \times \sum_{h',l'} b_{l'} D_{h'}^{l'} \sum_{h,l} b_l^* D_h^{l*} X(\mathbf{Q},\mathbf{Q}',\varepsilon). \quad (6)$$

Here we have introduced the abbreviation

$$X(\mathbf{Q},\mathbf{Q}',\varepsilon)=\sum_i p_i \sum_f \left\langle f\left|\int d^3r e^{i\mathbf{Q}\cdot\mathbf{r}} V(\mathbf{r}-\mathbf{R})\right|i\right\rangle \times\left\langle i\left|\int d^3r' e^{-i\mathbf{Q}'\cdot\mathbf{r}'} V(\mathbf{r}'-\mathbf{R}')\right|f\right\rangle \times\delta(\omega_{f,i}-\varepsilon), \quad (7)$$

where the vectors in reciprocal space,

$$\mathbf{Q}=\mathbf{k}_{0g}^j-\mathbf{k}_h^{l*},$$

$$\mathbf{Q}'=\mathbf{k}_{0g'}^{j'*}-\mathbf{k}_{h'}^{l'}, \quad (8)$$

have been used for convenience. The complex conjugates $\mathbf{k}_h^{l*}$ and $\mathbf{k}_{0g'}^{j'*}$ have been obtained from $\langle\mathbf{k}|\mathbf{r}\rangle=\exp(-\mathbf{k}^*\mathbf{r})$. In case of vanishing absorption, as assumed in the following, this is of no importance.

We will henceforth omit constant prefactors in expressions for the differential cross section. This is justified since in experiments intensities are in general not normalized. $\mathbf{R},\mathbf{R}'$ are position operators of the target that is described in the one-electron approximation (justified since core excitations are essentially one-electron excitations).[3] The integrals in Eq. (7) can be taken as Fourier transforms of the Coulomb potential which are proportional to Q^{-2}. From the shift theorem we have

$$X(\mathbf{Q},\mathbf{Q}',\varepsilon)=\frac{4\pi e^2}{Q^2Q'^2}\sum_i p_i\sum_f \langle f|e^{i\mathbf{Q}\cdot\mathbf{R}}|i\rangle \times\langle i|e^{-i\mathbf{Q}'\cdot\mathbf{R}'}|f\rangle\delta(\omega_{f,i}-\varepsilon). \quad (9)$$

Note that for ease of writing the indices g,h,j,l, g',h',j',l' of the reciprocal vectors $\mathbf{Q},\mathbf{Q}'$ that appear as arguments in X have been omitted. What has been achieved with Eq. (6) seems at first glance to be nothing than a separation into prefactors a,b,C,D that depend only on the orientation of the source and the detector relative to the crystal, and factors $X(\mathbf{Q},\mathbf{Q}',\varepsilon)$ that depend on the scattering properties of the medium. When the incident electron can be described by an N-beam case, and the outgoing one by an M-beam case, the expression (6) for the cross section contains $(NM)^4$ terms, and so even for a two-beam in–two-beam out case, we have to deal with 256 terms. For usual systematic-row conditions, one can easily arrive at 10^5 terms.

B. Mixed dynamic form factor

A closer inspection of the factors X will show that a number of terms in Eq. (6) vanish, and many of the remaining ones can be collected before evaluating the sum; for the two-beam case the sum reduces, eventually, to a linear combination of six different X.

First we note that the mixed dynamic form factor[23] $S(\mathbf{Q},\mathbf{Q}',\varepsilon)$ is defined as

$$S(\mathbf{Q},\mathbf{Q}',\varepsilon)=\sum_i p_i\sum_f \langle f|e^{i\mathbf{Q}\cdot\mathbf{R}}|i\rangle \times\langle i|e^{-i\mathbf{Q}'\cdot\mathbf{R}'}|f\rangle\delta(\omega_{f,i}-\varepsilon). \quad (10)$$

whence from Eq. (9)

$$X(\mathbf{Q},\mathbf{Q}',\varepsilon)=\frac{4\pi e^2}{Q^2Q'^2}S(\mathbf{Q},\mathbf{Q}',\varepsilon). \quad (11)$$

We make now use of certain properties of S. As has been shown by Kohl and Rose[23] the mixed dynamic form factor in an infinitely large crystal vanishes except that

$$\mathbf{Q}'=\mathbf{Q}+\mathbf{G}. \quad (12)$$

The arguments in S must differ by a reciprocal lattice vector $\mathbf{G}$.[30]

When the wave-vector differences $\mathbf{k}_{0g}^j-\boldsymbol{k}_h^l$ of the fast electron before and after scattering are expressed as usual by deviations of the dispersion surfaces from the sphere[28] γ^j and lattice vectors $\mathbf{g}$ (see Fig. 1), we can write Eqs. (8) as

$$\mathbf{Q}=\mathbf{k}_{0g}^j-\mathbf{k}_h^l=\mathbf{q}+\delta\gamma^{jl}\hat{\mathbf{k}}_z+\mathbf{g}-\mathbf{h}, \quad (13a)$$

$$\mathbf{Q}'=\mathbf{k}_{0g'}^{j'}-\mathbf{k}_{h'}^{l'}=\mathbf{q}+\delta\gamma^{j'l'}\hat{\mathbf{k}}_z+\mathbf{g}'-\mathbf{h}'. \quad (13b)$$

Here we have introduced the momentum transfer $\mathbf{q}$ between the incident ($\mathbf{k}_0$) and measured ($\mathbf{k}$) plane waves. The differences of *Anpassungen* are vectors in the z direction (unit vector $\hat{\mathbf{k}}_z$) with modulus

$$\delta\gamma^{jl}=(\gamma_i^j-\gamma_f^l), \quad (14)$$

and $\gamma_{i,f}^j$ is the deviation of the jth dispersion surface of the initial and final fast-electron waves from the sphere, as defined in the theory of dynamical diffraction.[28] All γ^j are functions of the deviation parameters w_i,w_o of the incident and the outgoing waves, respectively, and hence of $\mathbf{k}_0,\mathbf{k}$. The deviation parameter for the incident wave is $w_i=s_i\xi_g$ where ξ_g is the extinction distance for the g-reflex in question, and the excitation error is given by $s_i=|\mathbf{G}|\vartheta$, where ϑ is the tilt angle relative to the exact Bragg orientation, and analogous w_o for the outgoing (detected) wave. In the two-beam case, the reciprocal lattice vectors $\mathbf{g},\mathbf{h},\mathbf{g}',\mathbf{h}'$ are vectors of the systematic row. Equation (13), inserted into Eq. (12), yields now for the z component

$$\delta\gamma^{jl}=\delta\gamma^{j'l'}+|\mathbf{g}_z| \quad (15)$$

and $\mathbf{g}_z$ is a reciprocal lattice vector in the z direction. Since $\gamma<<G$, it follows that $\delta\gamma^{jl}=\delta\gamma^{j'l'}$, a condition fulfilled when $j=j'$ and $l=l'$.

C. Equivalence to the independent Bloch-wave model

This is an important result. There are four types of transitions $j \rightarrow l$ between branches 1 and 2 of the dispersion surface: $1 \rightarrow 1$ and $2 \rightarrow 2$ are intrabranch transitions, $1 \rightarrow 2$ and $2 \rightarrow 1$ are interbranch transitions. Equation (15) shows that different transitions do not interfere. This is equivalent to the independent Bloch-wave model (IBWM).[19] In fact, if the initial and final states are mixtures of both types of BW's, the total probability is given by the sum over the four terms given above. In other words, for a thick crystal inelastic scattering can be calculated within an IBWM as noted by Wright and Bird.[19]

A closer inspection of Eq. (15) shows that for a singular value of q, namely, $q_x=0$, interference terms ($j \neq j'$) exist when $j=l, j'=l'$, even for $d \rightarrow \infty$. d is the specimen thickness. For finite d, these terms cause a thickness-dependent oscillation next to zero scattering angle. This shows that the off-diagonal density matrix elements are not really damped out, and that the phase is not really erased. The vanishing of interference terms between Bloch waves means that off-diagonal terms of the density matrix of the fast electron vanish in a Bloch-wave basis. That is, the effect of the phases of the incident particle has been erased. Whereas usually the off-diagonal terms are damped by absorptive processes,[32] it is momentum conservation in the z direction that is responsible for the damping in the present case, and thus for the validity of the IBWM. For finite thickness, the mixed dynamic form factor $S(\mathbf{Q},\mathbf{Q}',\varepsilon)$ would have an envelope proportional to[36] $\Sigma_{jl,j'l'} \sin[(\delta\gamma^{jl}-\delta\gamma^{j'l'})d/2]/[(\delta\gamma^{jl}-\delta\gamma^{j'l'})d/2]$. It follows that condition (15) is relieved, allowing interference terms between Bloch waves. Momentum conservation is then only approximately valid due to resonance errors in the z direction.[33] A calculation of the additional terms shows that important features of the ESD pattern, such as the interference term, or the shift of the main maximum, remain virtually unchanged. This is the scope of a forthcoming paper.

It would be interesting to measure the inelastic cross section for intermediate crystal thickness in order to get insight into the strength of decoherence effects caused by the missing phase relations between Bloch waves in the IBWM. In elastic scattering, decohering is much more difficult to observe because in thicker crystals the oscillation period of the interference term (the rocking curve) is very small, and so is the amplitude.

Only when absorption is included will this oscillating contribution that approaches a δ function disappear.

D. Final expression

As discussed in Sec. I, we put $d \rightarrow \infty$. This fact reduces the number of terms in Eq. (6) to $(NM)^3$, in the two-beam case to 64.

Since $j=j', l=l'$, Eq. (6) is now

$$\frac{\partial^2\sigma}{\partial\varepsilon\,\partial\Omega} \propto \sum_j \sum_l \sum_{g,g',h,h'} a_j C_g^j a_j^* C_{g'}^{j*} b_l D_h^l b_l^* D_{h'}^{l*} \times X(\mathbf{q}+\delta\gamma^{jl}\hat{\mathbf{k}}_z+\mathbf{g}-\mathbf{h},\mathbf{q}+\delta\gamma^{jl}\hat{\mathbf{k}}_z+\mathbf{g}'-\mathbf{h}',\varepsilon). \tag{16}$$

For ease of writing, we define $X_{gh}(\mathbf{q},\varepsilon)=X(\mathbf{q}+\mathbf{g},\mathbf{q}+\mathbf{h},\varepsilon)$.

The dynamic form factors are almost constant in the small range where the differences of γ vary, and so

$$X(\mathbf{q}+\delta\gamma\hat{\mathbf{k}}_z+\mathbf{g},\mathbf{q}+\delta\gamma\hat{\mathbf{k}}_z+\mathbf{h},\varepsilon) \approx X_{gh}(\mathbf{q},\varepsilon). \tag{17}$$

We can now regroup the sums in Eq. (6) as

$$\frac{\partial^2\sigma}{\partial\varepsilon\,\partial\Omega} \propto \sum_{gg'} \sum_{hh'} A_{gg'} B_{hh'} X_{g-h,g'-h'}(\mathbf{q},\varepsilon), \tag{18}$$

with

$$A_{gg'} = \sum_j |a_j|^2 C_g^j C_{g'}^{j*},$$

$$B_{hh'} = \sum_l |b_l|^2 D_h^{l*} D_{h'}^l. \tag{19}$$

There are $(NM)^2$ terms in Eq. (18) to be calculated from the expansion coefficients of the incident and outgoing Bloch waves,[17] 16 in the two-beam case.

By changing the summation index $g-h=g_1$, $g'-h'=g_2$ and rearrangement with respect to different $X_{g,h}$, the number of terms can still be reduced,

$$\frac{\partial^2\sigma}{\partial\varepsilon\,\partial\Omega} \propto \sum_{g_1=-M+1,g_2=-M+1}^{N-1,N-1} F_{g_1g_2} X_{g_1g_2}(\mathbf{q},\varepsilon), \tag{20}$$

where

$$F_{g_1g_2} = \sum_{hh'} A_{g_1+h,g_2+h'} B_{hh'}. \tag{21}$$

Equation (20) has $(N+M-1)^2$ terms, which in the two-beam–two-beam case is 9.

III. SIMPLIFICATIONS

A. Two-beam case

In the two-beam-case, the various combinations of g and h (0 or G) lead to a set of nine different X_{gh}, namely, $\{X_{gh}|g=\{-G,0,G\},h=\{-G,0,G\}\}$. Assuming that the crystal is centrosymmetric and invariant under time reversal[23] we have $S(\mathbf{q},\mathbf{q}',\omega)=S(\mathbf{q}',\mathbf{q},\omega)$, and hence $X_{gh}(\mathbf{q})=X_{hg}(\mathbf{q})$. This symmetry property reduces the number of terms again. For discussion, it is useful to distinguish direct terms ($g=h$) and mixed terms ($g \neq h$). There are $L=M+N-1$ direct terms and $L(L-1)/2$ mixed terms. In the two-beam case, that makes three direct and three mixed terms.

The direct terms are the usual double differential cross sections, centered at the Bragg spots $-\mathbf{G},\mathbf{0},\mathbf{G}$ and would have been obtained likewise from a kinematical approach.

The mixed terms correspond to the nondiagonal elements of the mixed dynamic form factor. They are caused by the interference of waves belonging to Bragg reflexions G and 0.

When there were a one-beam case incident (far from the Bragg condition) and two outgoing beams, or vice versa, we would have $L=2$ direct terms and $L(L-1)/2=1$ interfer-

ence term. This corresponds to the double-slit experiment, the two beams being waves from the slits, and the single beam being the source.

The prefactors of the six terms can be calculated from dynamical theory, choosing directions of the incident and the outgoing electrons, from Eqs. (19), (21). There are obviously two parameters, namely, the directions of incident and of outgoing electrons, and they can conveniently be expressed by the deviation from the Bragg conditions w_i and w_o of the incident and outgoing waves, where $w=s\xi_g$. See Fig. 1 for a visualization of the notation we use.

Starting from expressions for C_g^j, D_h^l, e.g.,[28] Eqs. (19), (21), yield

$$F_{00}=1+\frac{2-v_i-v_o+2w_iw_o}{v_iv_o},$$

$$F_{gg}=\frac{v_o-1}{v_iv_o}, \tag{22}$$

$$F_{-g-g}=\frac{v_i-1}{v_iv_o}$$

for the direct terms and

$$F_{0g}=-\frac{2[w_o+w_i(v_o-1)]}{v_iv_o},$$

$$F_{0-g}=-\frac{2[w_i+w_o(v_i-1)]}{v_iv_o}, \tag{23}$$

$$F_{g-g}=-\frac{2w_iw_o}{v_iv_o}$$

for the mixed terms. Here we used the abbreviation

$$v_{i,o}=2(1+w_{i,o}^2). \tag{24}$$

These quantities are plotted in Fig. 2 as functions of w_i and w_o.

B. Dipole approximation

We have already made use of certain properties of the mixed dynamic form factor S as defined in Eq. (10). In a crystal, one-electron eigenfunctions $|i\rangle$ and $|f\rangle$ can only be calculated to some approximation. As has been argued on intuitive grounds,[34] atomic wave functions can be used for the initial state. Using spherical waves for the ejected electron, the mixed dynamic form factor can be calculated to good approximation.[35] It is well known that the ordinary dynamic form factor for ionization of free atoms can well be described within the dipole approximation, with an accuracy of the order of 10% in the angular integrated cross section.[25] We make use of these two approximations (free atoms and dipole) and write for the mixed dynamic form factor[23]

$$S(\mathbf{Q},\mathbf{Q}',\varepsilon)=f(\varepsilon)\mathbf{Q}\mathbf{Q}', \tag{25}$$

where $f(\varepsilon)$ shall be set constant since we consider a particular energy loss.

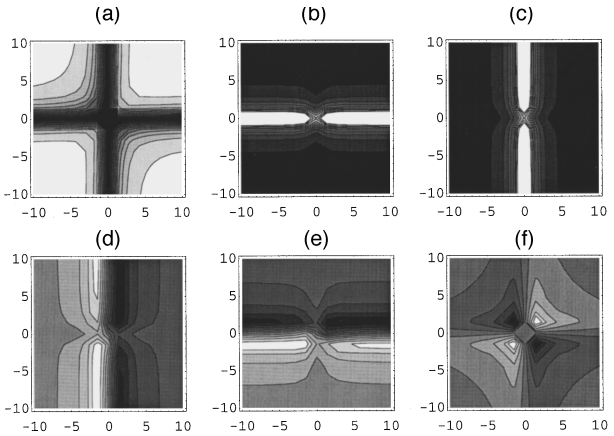

FIG. 2. Contour plots of the prefactors $F_{gh}(w_o,w_i)$: horizontal, w_o; vertical, w_i. The upper row, from left to right (a)–(c) shows the three direct terms F_{00} (defect line), F_{gg}, F_{-g-g} (excess line), the lower row (d)–(f) is for the three mixed ones F_{g0} (excess band), F_{-g0}, F_{-gg}.

With this expression, the direct terms X_{gg} in the cross section Eq. (20) lead to Lorentzians centered at the Bragg reflections $G,0,-G$, as explained above. An important consequence is that the mixed terms $X_{gh}(\mathbf{q},\varepsilon)$ become negative in a circular region around the midpoint between g and h in the diffraction plane. This has already been realized by Gjønnes,[21] but seems to have gone unnoticed later on.

We are now prepared to calculate the direct and mixed contributions to the ionization cross section, Eq. (20).

IV. DISCUSSION

The following contour plots and graphs have been calculated for a Si 220 two-beam case.[31] The energy loss is assumed to be the Si K-edge ionization loss at 1840 eV. The relation between the excitation errors of the incident and outgoing beams and $\mathbf{q}$ can be seen in Fig. 1. For Si (220), we have

$$\frac{q_x}{q_G}=\frac{(w_o-w_i)}{6.52}. \tag{26}$$

We present scattering profiles and contour plots as functions of w_i, w_0 in order to make relations to Kikuchi patterns.

In Fig. 2 we show the prefactors of the three direct terms [Figs. 2(a)–2(c)] and the three mixed terms [Figs. 2(d)–2(f)], as contour plots over parameters w_o and w_i. w_o is on the horizontal axis. For kinematical conditions (large w_i) the incident wave can be considered to be plane. This is the case that Kainuma[3] discussed without reference to particular energy losses or to a specific S. Kainuma's expressions for bands and lines can be found in Fig. 2 as a scan at very large w_i. Figure 2(a) constitutes the defect line, and Fig. 2(c) has the shape of an excess line but is not strong enough to compensate the defect line when the incident beam is nearer to the 220 Kikuchi line ($-w_i<3.26$); else it causes an excess line. The Kikuchi band is shown in Fig. 2(d). Note that it is

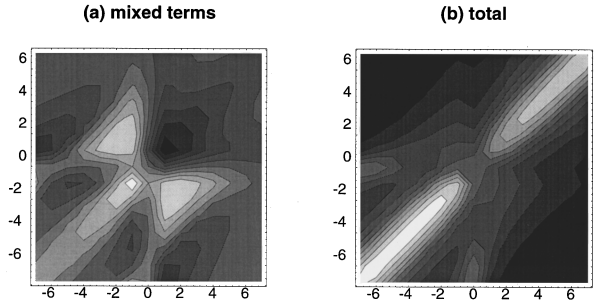

FIG. 3. (a) Mixed terms in the inelastic scattering cross section, for Si 220 two-beam case and the Si K edge. Intensity along the systematic row ($q_y=0$), as a function of w_0 (horizontal), and w_i (vertical). (b) Total (direct plus mixed terms) inelastic scattering cross section, for Si 220 two-beam case and the Si K edge. Intensity along the systematic row ($q_y=0$), as a function of w_0 (horizontal), and w_i (vertical).

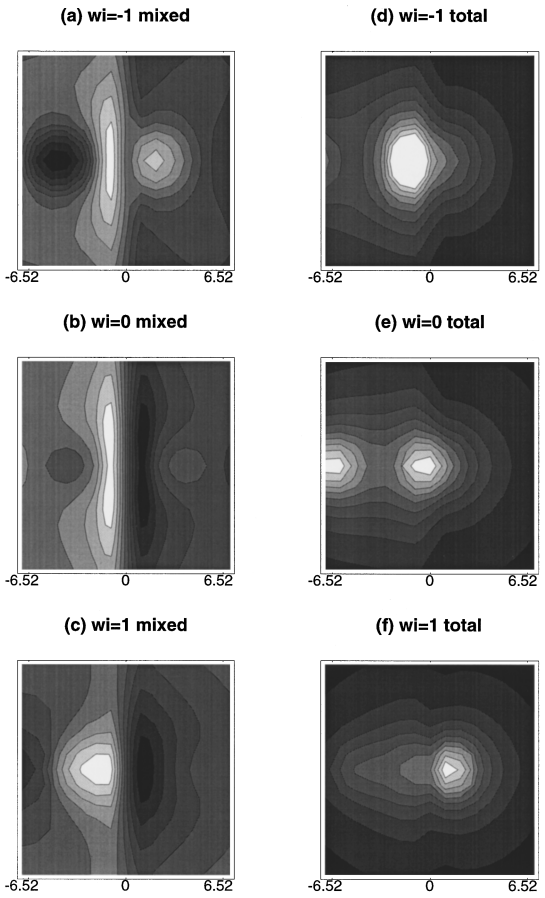

FIG. 4. (a)–(c) Mixed contribution to the Si K-edge ESD pattern for $w_i=-1,0,1$ (top to bottom). Horizontal axis given in units of w_o, vertical axis given in units of the Bragg vector, drawn to scale. The Bragg spot is at $w_o=-6.52, q_y=0$. (d)–(f) Si K-edge ESD pattern, total intensity, same parameters as in Figs. 4(a)–4(c).

an excess band when $S(\mathbf{q},\mathbf{q}',\varepsilon)>0$. We shall see shortly that this is not always the case. The other prefactors are not given by Kainuma who has only two direct [Figs. 2(a), 2(c)] and one mixed [Fig. 2(d)] term. In fact, for large w_i the terms of Figs. 2(b), 2(e), and 2(f) tend to a constant, and there remain only the terms discussed by Kainuma for the kinematical case. In the present representation, the dynamical case is included in a natural way, and the symmetry between incident and outgoing beams is seen most clearly. Compare Fig. 2(b) and Fig. 2(c): A rocking curve with fixed detector position is identical to a scan over the diffraction pattern with fixed incident beam. As an aside, we mention that the direct term F_{00} — the defect line — is asymmetric for moderate w_i.

The lower row shows bandlike contributions. They are all antisymmetric with respect to w_i or w_o. Note that in usual reasoning, only the term of Fig. 2(d) is discussed.

The relative weight of the six terms depends on the mixed dynamic form factor. In order to discuss linelike and bandlike structures in more detail, we calculate the inelastic cross section along the line joining the incident beam and the G spot, as a function of w_o and w_i. This is shown in Fig. 3(b). Note that along the diagonal the scattering angle is zero. Or, for given w_i, the angular profile is a horizontal cut through the contour plot with the origin at $w_i=w_o$. The momentum transfer in direction of the systematic row is given by Eq. (26).

Figure 3(a) shows the sum over the three mixed terms — in usual notation the Kikuchi band. It can be clearly seen that the intensity distribution is not bandlike. A horizontal cut through the ''butterfly'' is bandlike for $w_i>0$. For $-1<w_i<0$, a cut shows more structure, with two maxima, one inside and one outside of the former band, and a significant decrease of intensity in the band. For smaller w_i the contrast reversal is more pronounced.

This shows that the usual notation of a Kikuchi band is a useful, but not exact description of the situation. The contrast reversal from excess to defect, seen here, is usually masked by the strong Lorentzian direct terms. It should also be noted that this should not be mistaken for the contrast reversal of the band in thicker specimens.[2]

The direct terms are much more intense than the mixed ones. The main contribution is a Lorentzian centered at the incident beam (the diagonal of the graph). Figure 3(b) shows the total intensity (direct plus mixed terms). The linelike and bandlike structures are barely visible because the Lorentzian is so dominant.

The excess Kikuchi line begins to emerge at the lower part of the contour plot as a slight structure for $w_o\approx 0$. Note the appearance of a subsidiary maximum when $w_i=-6.52$. It can also be seen that the cross section is higher for $w_i<0$ than for $w_i>0$.

Figure 4(a) shows energy filtered diffraction patterns [energy spectroscopic diffraction (ESD)]. Figures 4(a)–(c) are the mixed contributions to the K-edge ESD pattern for three different excitation errors. For $w_i=0$ (exact Bragg case) or $w_i=1$ the excess band is strong and well defined. For $w_i=-1$ the contrast is reversed around a circular area centered at the midpoint between the incident beam and the G reflection, as already predicted by Gjønnes,[21] see also remark given above. The total ESD intensity distribution is shown in Figs. 4(d)–4(f). The Lorentzian direct term dominates the pattern except for large distance from the systematic row

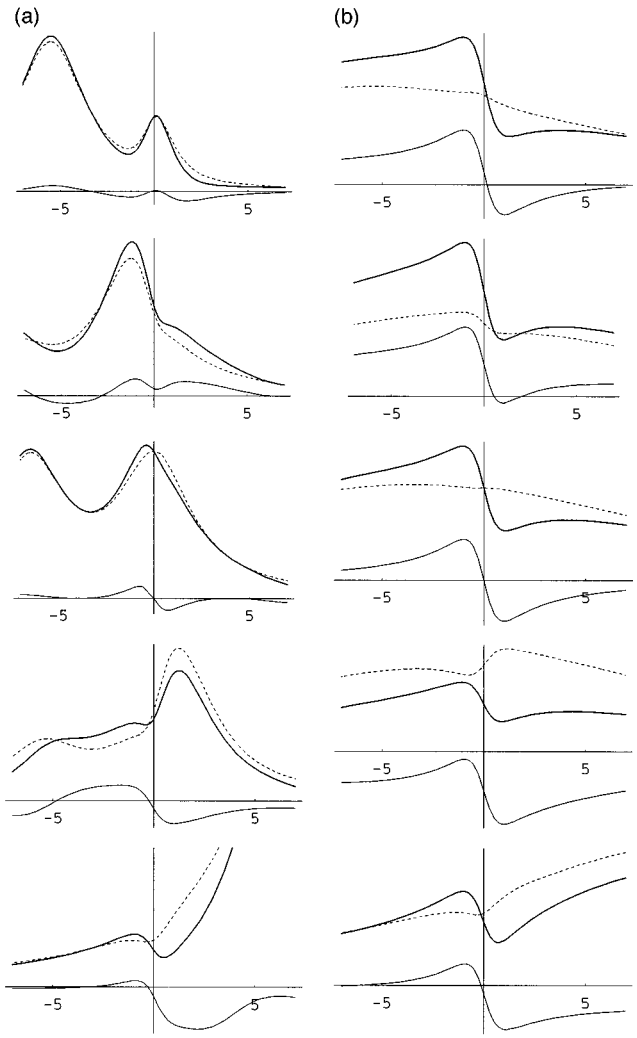

FIG. 5. (a) Traces through Si K-edge ESD pattern along $0G$ $(q_y=0)$. Direct term (dashed line), mixed (thin solid line), and total inelastic cross section. From top to bottom: $w_i=-5.52$, -1, 0, 1, 10. Abscissa: w_o. (b) Traces through Si K-edge ESD patterns parallel to $0G$ $(q_y=2)$. Direct term (dashed line), mixed (thin solid line), and total inelastic cross section. From top to bottom: $w_i=-5.62, -1$, 0, 1, 10. Abscissa: w_o.

where the excess Kikuchi band becomes visible. The defect region visible in Fig. 4(a) is hidden by the direct term and disappears in the total ESD pattern, Fig. 4(d). A comparison with Fig. 4(e) shows, however, that the minimum between the excited Bragg reflection $-G$ and the incident beam is lower. This depression has been seen experimentally.[36]

Figure 5 shows various traces through the ESD pattern. The left column is a trace along $0G$ $(q_y=0)$; the right column is a trace parallel to $0G$ at a distance of two Bragg angles $(q_y=2)$. Along $0G$ the Kikuchi line and band is barely visible since the Lorentzians dominate, as already mentioned. From top to bottom, the excitation error of the incident beam is increased. The top is for $w_i=-5.52$ (corresponds to $w_i=-1$ for the $\overline{220}$ Kikuchi line). In the second graph, we have put $w_i=-1$. There we have contrast reversal in the band (thin line) as already discussed in Fig. 4, causing a narrowing of the left wing of the Lorentzian and a dip at the position of the Kikuchi line. The direct terms are almost Lorentz-like. At $w_i=0$ (third from top) the bandlike contribution shifts the maximum to the left. An important consequence is that, in ESD patterns, the center points of the Lorentzians must not be taken as positions of the Bragg spots. For $w_i=1$ the band is strong. The last graph resembles kinematical conditions $(w_i=10)$.

The right columns (two Bragg reflections away from the systematic row) shows the excess band more clearly. Note that it is strongest for negative w_i. At $w_i=1$, the defect Kikuchi line (dashed) counteracts the band, making it faint. The linelike structure in the direct term is a small effect. For $w_i=-5.52$ — incident beam next to the G position, equivalent to $w_i=-1$, and detection at the $\overline{220}$ -Kikuchi line — we observe an excess line that is hidden by the strong Lorentzian profile when $q_y=0$ and hidden by the excess band for large q_y. For $-w_i<3.26$ we have a defect line, as expected.

It is at once evident that the usual notion of Kikuchi bands and lines is an approximation for larger distances from the excited beams $(q_y>>0)$ and for kinematical conditions $(|w_i|>>1)$. In ESD patterns of inner-shell ionization, intensity is concentrated in the direct terms around the excited spots, rendering the indirect bandlike contribution faint along the excited systematic row. The contrast reversal seen for $w_i=-1$ is compensated by the relatively large direct term, anyway causing a decrease of intensity between 0 and G. This effect has been observed in preliminary experiments with an imaging filter.[36]

The fact that both the line and the band are small effects compared to the Lorentzian distribution of the inner-shell ionization justifies the usual kinematical interpretation of ESD patterns invoking superposed Lorentzians, and this is the very reason why EELS quantitation works, in general.

Accurate microanalysis demands, however, more involved reasoning. As shown in a model calculation,[12] the cross section may change by a factor of 10, under particular conditions, as a function of crystal orientation. The method developed here serves as a tool for estimating the effects of orientation on the cross section. Of special interest is the case of site-specific excitations, which can also be handled with our approach. In order to see if and when simple formulas apply, and to find correction algorithms for more accurate EELS quantitation, it is necessary to extend our findings to a many-beam case and to include the thickness dependence as well as absorption. This is the aim of a following paper.

V. CONCLUSION

We point out the central benefit of the simplified model: Simulations of energy-filtered diffraction patterns can be done easily on a PC, thus allowing fast IBWM calculations for any two-beam case and any ionization edge.

Within the range of validity of the IBWM, the theory as outlined above, based on a fully dynamical expression, leads to a clear distinction between bandlike and linelike structures in ESD patterns.

Besides the excess and defect Kikuchi lines and the Kikuchi band, we find three further contributions that establish the complete symmetry between incident and outgoing waves.

The symmetry properties of the mixed dynamic form factor allow a considerable reduction of terms, and in the two-beam case we are left with six terms.

The model calculation for the Si K-ionization edge in the (220) two-beam case demonstrates interesting details in ESD patterns. Most important is the depression of the interpeak minimum, rendering a superposition of Lorentzians impossible. The shift of the maximum of the double-differential cross section relative to the Bragg spot must be considered when energy-filtered diffraction patterns are quantitatively interpreted.

Note added in proof. The results are accurate as long as the two-beam case is a good approximation, i.e., for $|w_{i,0}|<6.5/2$. For larger $|w|$, certain features are missing, such as the symmetry of the band.

ACKNOWLEDGMENTS

P. S. acknowledges the hospitality and the financial support of École Centrale Paris and of the Austrian Fond zur Förderung der wissenschaftlichen Forschung, Project No. P09631.

*On leave from Institut für Angewandte und Technische Physik der TU Wien, A-1040 Vienna, Austria.

[1] F. Hofer and P. Golob, Micron Microsc. Acta **19**, 73 (1988).

[2] L. Reimer, Adv. Electron. Electron Phys. **81**, 43 (1991).

[3] Y. Kainuma, Acta Crystallogr. **8**, 247 (1955).

[4] S. Takagi, J. Phys. Soc. Jpn. **13**, 278 (1958).

[5] S. Takagi, J. Phys. Soc. Jpn. **13**, 287 (1958).

[6] P. Rez, C.J. Humphreys, and M.J. Whelan, Philos. Mag. **35**, 81 (1977).

[7] C.J. Rossouw, Ultramicroscopy **16**, 241 (1985).

[8] Z.L. Wang, *Elastic and Inelastic Scattering in Electron Diffraction and Imaging* (Plenum, New York, 1995).

[9] C.J. Rossouw and M.J. Whelan, Ultramicroscopy **6**, 53 (1981).

[10] L.J. Allen, Ultramicroscopy **48**, 97 (1993).

[11] W. Coene and D. Van Roost, Ultramicroscopy **33**, 261 (1990).

[12] A. Weickenmeier and H. Kohl, Philos. Mag. B **60**, 467 (1989).

[13] R. Howie, Proc. R. Soc. London A **271**, 268 (1963).

[14] H. Yoshioka, J. Phys. Soc. Jpn. **12**, 618 (1957).

[15] P. Rez, in *Electron Diffraction 1927-1977*, edited by P. J. Dobson, J. B. Pendry, and C. J. Humphreys, IOP Conf. Proc. No. 41 (Institute of Physics and Physical Society, London, 1978), p. 61.

[16] C. Van Roost and R. Serneels, Philos. Mag. **56**, 397 (1987).

[17] This same expression is obtained when Bloch waves are inserted for ψ_{k_0}, ψ_k in Eq. (21) of Ref. 18.

[18] S.L. Dudarev, L.M. Peng, and M.J. Whelan, Phys. Rev. B **48**, 13408 (1993).

[19] A.G. Wright and D.M. Bird, Acta Crystallogr. Sect. A **45**, 342 (1989).

[20] F.N. Chukhovskii, L.A. Alexanjan, and Z.G. Pinsker, Acta Crystallogr. Sect. A **29**, 38 (1973).

[21] J. Gjønnes, Acta Crystallogr. **20**, 240 (1966).

[22] P. Schattschneider, *Fundamentals of Inelastic Electron Scattering* (Springer-Verlag, New York, 1986).

[23] H. Kohl and H. Rose, Adv. Electron. Electron Phys. **65**, 173 (1985).

[24] R.F. Egerton, *Electron Energy-Loss Spectroscopy in the Electron Microscope* (Plenum Press, New York, 1986).

[25] S.T. Manson, Phys. Rev. A **6**, 1013 (1972).

[26] S.L. Dudarev, L.-M. Peng and M.J. Whelan, Proc. R. Soc. London A **440**, 567 (1993).

[27] This important theorem is due to A. Sommerfeld. We obtained Eq. (4) in correct form by a propagator calculation without resorting to this theorem.

[28] L. Reimer, *Transmission Electron Microscopy*, Springer Tracts in Optical Sciences (Springer, Berlin, 1989).

[29] P.A. Stadelmann, Ultramicroscopy **21**, 131 (1987).

[30] It will turn out in the next subsection that this condition is equivalent to the IBWM. As shown by Wright and Bird (Ref. 19) deviations from the IBWM become important for thickness smaller than $\approx$100 nm in a Si-220 case. This is consistent with our estimates (Ref. 36).

[31] MATHEMATICA has been used. The source code is available from the authors on request.

[32] Yu. Kagan and Yu. Kononets, Zh. Éksp. Teor. Fiz. **64**, 1042 (1973) [Sov. Phys. JETP **37**, 530 (1973)].

[33] A.P. Young and P. Rez, J. Phys. C **8**, L1 (1975).

[34] D.K. Saldin, Philos. Mag. B **55**, 481 (1987).

[35] R.D. Leapman, P. Rez, and D.F. Mayers, J. Chem. Phys. **72**, 1232 (1980).

[36] M. Nelhiebel, Diploma thesis, Technical University, Vienna, 1995.